Energy Reports 8 (2022) 12348–12356

Contents lists available at ScienceDirect

Energy Reports

journal homepage: www.elsevier.com/locate/egyr

Research paper

Exergetic analysis of a continuous plant for the hydrothermal reduction of CO_2 into formate

Laura Quintana-Gómez [a], José J. Segovia [b], Ángel Martín [a,*], M. Dolores Bermejo [a]

[a] BioEcoUva. Research Institute on Bioeconomy, PressTech Group, Department of Chemical Engineering and Environmental Technology, Universidad de Valladolid, Doctor Mergelina s/n, 47011, Valladolid, Spain

[b] BioEcoUva. Research Institute on Bioeconomy, Laboratory of Thermodynamic and Calibration TERMOCAL, Department of Energy and Fluid Mechanics Engineering, Universidad de Valladolid, Paseo de Belén s/n, 47011, Valladolid, Spain

ARTICLE INFO

Article history:
Received 10 June 2022
Received in revised form 25 August 2022
Accepted 14 September 2022
Available online 28 September 2022

Keywords:
CO_2 utilization
Exergy analysis
Exergy destruction
Exergoeconomic analysis

ABSTRACT

Carbon capture and utilization can mitigate the problems caused by CO_2 emissions, at the same time that valuable products are obtained from the conversion of CO_2. By reduction of CO_2 in hydrothermal conditions (T = 275°C, P = 200 bar), high yields of conversion of CO_2 to formate of up to 70% can be achieved in reaction times of 1 h. This technology can be implemented as a continuous process in large CO_2 production sites, and for this purpose the energy optimization of the process is essential to make it technically and economically feasible. Therefore, the objective of this work is to evaluate the thermodynamic efficiency and the cost of the different units involved in the hydrothermal conversion of CO_2 into formate. Exergy balances were applied to the main units of a continuous plant for the hydrothermal reduction of CO_2 into formate. The exergy efficiency, exergy improvement potential rate, the exergoeconomic costs and the sustainability index were calculated along with the exergy destruction rate in the main process units. The specific exergy destroyed per kg of formate produced was calculated as 6260 kJ/kg. The results showed that the major exergy destruction rate took place in the reactor, representing the 69% of the total exergy destruction in the plant. Although this destruction rate increased with the conversion in the reactor, in terms of the overall efficiency and exergetic cost of the process, a high conversion above 70% is advisable. The exergetic efficiency of each unit was also evaluated along with the exergetic improvement potential rate. The lowest efficiency was identified in the pump with a value of 0.44. In the case of the exergoeconomic performance, the reactor showed the highest cost rate representing the 67% of the total costs. The total exergoeconomic cost rate was 2.3 €/kg of formate produced.

1. Introduction

Anthropogenic emissions of carbon dioxide (CO_2) have continuously increased in the last century due to the combustion of fossil fuels, breaking the natural carbon cycle and contributing to a worldwide temperature rise due to its greenhouse potential (Alami et al., 2020; Anwar et al., 2020; Mac Dowell et al., 2017). This has stimulated investigations to reduce the atmospheric CO_2 by capturing it directly from air (Keith et al., 2018) or from power and chemical plants (De Guido et al., 2018).

Carbon capture and sequestration (CCS) techniques are generally based on the chemical absorption of CO_2 by aqueous solutions of amines or NaOH (Yoo et al., 2013; Yusuf et al., 2019) and the sequestration of the captured CO_2 into a geological storage. This process involves a high capital investment and operation costs, mainly related to the desorption step of the CO_2 in a stripping column and the compression of CO_2 through a multistage compression system prior to its transportation (Yusuf et al., 2019). Moreover, the value of CO_2 once stored underground is very limited or even null (Kothandaraman et al., 2016). Carbon capture and utilization (CCU) has arose as a potential alternative to overcome the drawbacks associated with CCS. In addition to the more favorable social perception of CCU compared to CCS due to the use of CO_2 rather than its storage, the conversion of the captured CO_2 into useful chemicals and fuels could compensate the high costs associated with CCS (Styring et al., 2011).

The direct conversion of CO_2 can be achieved by different methods, including hydrogenation, electrochemical reduction and photochemical reduction. The low yields and high costs associated with these techniques are the main concerns for their industrial application (Gomez et al., 2020). The catalytic hydrogenation of CO_2 is one of the most popular alternatives for CO_2 utilization

* Corresponding author.
E-mail addresses: mamaan@iq.uva.es (Á. Martín), mdbermejo@iq.uva.es (M.D. Bermejo).

https://doi.org/10.1016/j.egyr.2022.09.065

(Takahashi et al., 2008). However, gaseous H_2 is required and its production is associated with high energy consumption, as nowadays H_2 is mainly produced by the steam reforming of methane, which is an energy intensive process (Michalkiewicz and Koren, 2015). Additionally, the production of hydrogen from fossil fuels releases around 830 million tons of CO_2 per year (Jovan and Dolanc, 2020). Despite the advances in the past years to produce green hydrogen from renewable sources, these technologies are still not economically feasible (Jovan and Dolanc, 2020). Moreover, the use of hydrogen involves safety concerns, such as leakages and flammability (Gomez et al., 2020). To avoid the use of gaseous H_2, high-temperature water (HTW) has gained attention as a potential hydrogen donor and reaction media (Roman-Gonzalez et al., 2018). Additionally, the use of hydrothermal media enhances the economic feasibility of the integration of systems of capture and utilization of CO_2 eliminating the aforementioned high costs associated to the desorption of the CO_2.

Under hydrothermal conditions, CO_2 can be reduced to formic acid using Zn or other metals as reductants (Jin et al., 2014). Traditionally, formic acid has had important uses in industry such as preservative and insecticide. It is also a source of carbon in synthetic chemical industries and a useful reducing agent (Duo et al., 2016). Moreover, formic acid has attracted great interest as its potential use as a fuel or as a hydrogen storage vector in fuel cells (Mardini and Bicer, 2021).

In the past decades, exergy analysis has been established as a powerful tool to design and optimize energy-intensive manufacturing plants (Dincer and Rosen, 2020; Mojarab Soufiyan et al., 2016). Exergy analysis is based on the combination of the first and second law of thermodynamics and allows to determine the locations and causes of thermodynamic imperfections, as well as the quantities of energy loss or irreversibility (Aghbashlo et al., 2019; Dowlati et al., 2017; Mojarab Soufiyan et al., 2016). Exergy can be defined as the maximum amount of theoretical work that can be taken from a system as it reaches the equilibrium with its surroundings via reversible processes (Aghbashlo et al., 2019; Mojarab Soufiyan et al., 2017). Exergy measures the potential to produce change of a stream, taking the environment as the reference state (Terehovics et al., 2017).

Exergy analysis has been used to optimize a wide variety of chemical processes (Aghbashlo et al., 2019), such as food manufacturing plants (Dowlati et al., 2017; Mojarab Soufiyan et al., 2016, 2017), drying processes (Terehovics et al., 2017), combustion systems (Martín et al., 2006; Petrakopoulou et al., 2011; Xu et al., 2019), glycerol esterification with acetic acid (Aghbashlo et al., 2019) or in an industrial roller kiln to fire porcelain tiles (Ferrer et al., 2019), among other examples. The combination of exergy analysis with economic and environmental constrains results on exergoeconomic and exergoenvironmental evaluations which provide a more complete information for the optimization of plants (Aghbashlo et al., 2019).

To the authors' best knowledge, exergetic and exergoeconomic analysis have not been performed for the production of formate from CO_2. By performing this type of analysis, critical information with respect to the efficiency and the cost of the different steps involved in the hydrothermal conversion of CO_2 can be obtained. This information is important for the deployment of the technology because, considering the very large scale of the foreplaned CO_2 capture and conversion facilities, minimization of costs is essential. Therefore, this information, which is not available at the moment, can contribute to guide future research on this topic. Considering this, the aim of this work is to present a theoretical evaluation of the exergy balance in a continuous plant for the production of formate from CO_2 captured as $NaHCO_3$ under hydrothermal conditions. Moreover, this study presents the calculation of the exergetic efficiency of the process to quantify the exergy destruction along with the economic cost associated with this loss. The exergetic improvement potential rate and the sustainability index are also evaluated.

2. Description of the process

In a previous work of this research group (Quintana-Gómez et al., 2021), a continuous process for the hydrothermal conversion of CO_2 into formate was proposed. In the process described, 1000 kg/h of CO_2 was captured with aqueous NaOH, forming an aqueous solution of $NaHCO_3$ with a concentration of 1.2 M. The aqueous $NaHCO_3$ was reduced with Zn under hydrothermal conditions following the process described in the flow diagram of Fig. 1.

According to Fig. 1, the main steps in the hydrothermal reduction of CO_2 in the form of $NaHCO_3$ are:

(1) The feed solution of $NaHCO_3$ at 25 °C and 1 bar (stream 1) is pressurized to 200 bar in the pump (P-1). By pressurizing the solution before heating, it is ensured that water remains in the liquid state during the entire process, reducing loss of captured CO_2 to the gas phase and improving the reliability of the operation.
(2) After pressurizing the aqueous $NaHCO_3$, stream 2 is heated to 277 °C in the heat exchanger E-1. The temperature reached in unit E-1 was calculated taking into account that the mixture of the aqueous $NaHCO_3$ with the reductant Zn has to be introduced in the reactor at 275 °C.
(3) The hopper (TK-1) where Zn is stored is pressurized at 200 bar with N_2 to avoid the oxidation of Zn particles.
(4) Zn particles and aqueous $NaHCO_3$ are mixed through a three-way valve (V-1).
(5) The reduction of the $NaHCO_3$ solution into formate takes place in the reactor (R-1) according to reactions R1 and R3, consuming hydrogen produced by the oxidation of Zn with R2. According to the theoretical optimization of the process developed in a previous work of this research group (Quintana-Gómez et al., 2021), the optimum reaction conditions are a $Zn/NaHCO_3$ mole ratio of 1.5, pressure of 200 bar, temperature of 275 °C and a residence time of 60 min. Under these conditions, the yield to formate obtained in a continuous plug flow reactor was of 71%. H_2 is also formed during the reaction. It is considered that all the Zn is oxidized to ZnO. It must be noted that Zn is oxidized very rapidly according to reactions 1 and 2 (Jin et al., 2014; Roman-Gonzalez et al., 2018). Stream 6 is composed by the reaction products and the unreacted reactants.
(6) ZnO formed is completely separated in the hydrocyclone (S-1). Solids leave the hydrocyclone with a 20% of humidity (stream 7) while stream 8 is composed by the reaction products and unreacted $NaHCO_3$.
(7) After separating of the solids, stream 8 is cooled to 35 °C. In order to save energy, an energetic integration is carried out between stream 2 and stream 8 (Quintana-Gómez et al., 2021). Therefore, stream 8 is used to heat stream 2 to 277 °C in heat exchanger E-1, leaving this unit at 45 °C. To finish the cooling of stream 8, it is necessary to incorporate a cooler (C-1) which used 4000 kg/h of cooling water at 20 °C to complete the cooling of stream 8 down to 35 °C.
(8) Once the stream is cooled (stream 10), it is depressurized through the isenthalpic valve V-2.
(9) In the flash chamber (S-2), stream 11, composed by the products and unreacted $NaHCO_3$, is separated into its gaseous (stream 12) and liquid components (stream 13). To calculate the concentration of each component in the flash unit, it is considered that $NaHCO_3$ is decomposed in its equilibrium species (Quintana-Gómez et al., 2021).

The characteristics of each stream involved in the hydrothermal reduction of CO_2 in the form of $NaHCO_3$ into formate are

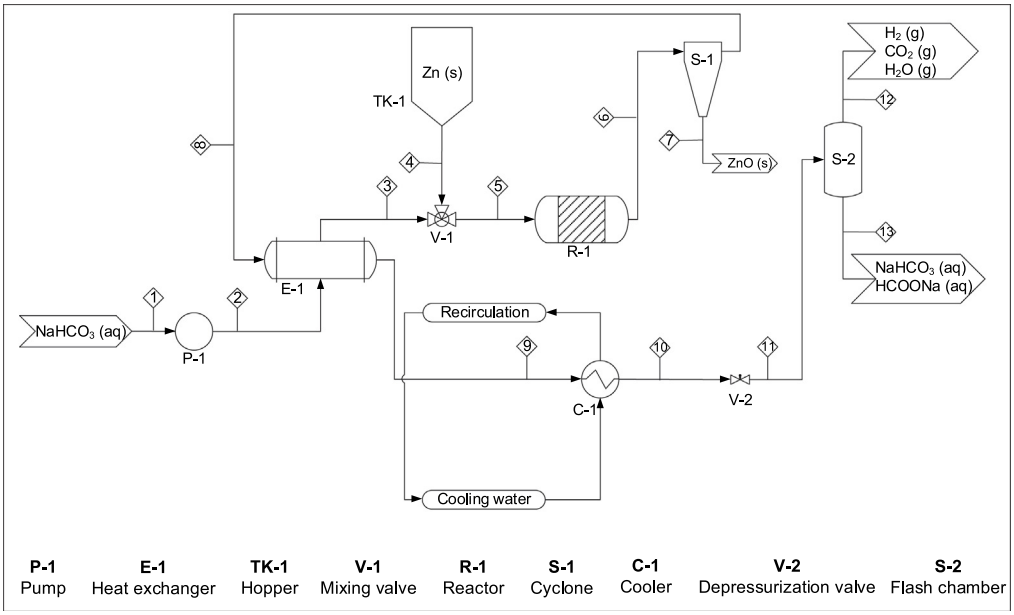

Fig. 1. Flow diagram of a continuous plant for the hydrothermal conversion of CO_2 (https://pubs.acs.org/doi/10.1021/acs.iecr.1c01961).
Source: Adapted and reprinted with permission from Quintana-Gómez et al. (2021),
© 2021 ACS Further permissions related to this material should be directed to the ACS.

detailed in Table 1, including its temperature, pressure and mass and energy balances.

$$HCO_3^-(aq) + Zn(s) \rightarrow HCOO^-(aq) + ZnO(s) \quad (R1)$$

$$H_2O(l) + Zn(s) \rightarrow H_2(aq) + ZnO(s) \quad (R2)$$

$$HCO_3^-(aq) + H_2(aq) \leftrightarrow HCOO^-(aq) + H_2O(l) \quad (R3)$$

3. Exergy analysis

To conduct the exergetic analysis of a continuous plant for the hydrothermal conversion of $NaHCO_3$ into formate, the following assumptions were considered:

- The conversion process was carried out under steady state conditions.
- Potential and kinetic exergies were considered negligible due to their small contributions to the overall exergy in comparison with physical and chemical exergy.
- Temperature and pressure of the environment taken as reference were 25 °C and 1 bar, respectively.
- The variations of the conditions of the surroundings were neglected.

The overall exergy balance for each unit of the proposed continuous plant is expressed in Eq. (1) (Aghbashlo et al., 2019):

$$\dot{E}_{in} + \dot{W} = \dot{E}_{out} + \dot{E}_Q + \dot{E}_D \quad (1)$$

where $\dot{E}_{in}$ is the rate of exergy supplied by the inlet stream (kW), $\dot{W}$ is the electrical work rate (kW), $\dot{E}_{out}$ is the rate of exergy supplied by the output stream (kW), $\dot{E}_Q$ is the exergy transfer rate during the heat lost to the surroundings (kW) and $\dot{E}_D$ is the exergy destruction rate, also called irreversibility rate ($\dot{I}$) (kW). The exergy transferred as heat from each unit to the surroundings ($\dot{E}_Q$) can be calculated by Eq. (2) (Dowlati et al., 2017):

$$\dot{E}_Q = \dot{Q}_l \left(1 - \frac{T_0}{T}\right) \quad (2)$$

where T_0 is the temperature of the environment and T the temperature of the surroundings. In this work, the surroundings of the system are coincident with the environment ($T_0 = T$). Therefore, the exergy transferred to the surroundings is null for all the units of the process and Eq. (1) can be rewritten as Eq. (3).

$$\dot{E}_{in} + \dot{W} = \dot{E}_{out} + \dot{E}_D \quad (3)$$

The exergy rate of the inlet and output mass flows includes different components. In the absence of nuclear effects, magnetism, electricity and surface tension, the exergy rate $\dot{E}$ is defined by Eq. (4) (Kotas, 2012).

$$\dot{E} = \dot{E}_k + \dot{E}_p + \dot{E}_{ph} + \dot{E}_{ch} \quad (4)$$

where $\dot{E}_k$ is the kinetic exergy (kW), $\dot{E}_p$ is the potential exergy (kW), $\dot{E}_{ph}$ is the physical exergy (kW) and $\dot{E}_{ch}$ is the chemical exergy (kW). Since $\dot{E}_k$ and $\dot{E}_p$ can be neglected in this study, Eq. (4) can be written as:

$$\dot{E} = \dot{E}_{ph} + \dot{E}_{ch} \quad (5)$$

In a liquid stream composed by the mixture of j substances, $\dot{E}_{ph}$ is calculated according to Eq. (6) (Kotas, 2012):

$$\dot{E}_{ph} = \sum_j \dot{m}_j \left(H_j - H_0\right) - T_0 \left(S_j - S_0\right) \quad (6)$$

where $\dot{m}_j$ is the mass flow rate (kg/s) of the jth component, H_j and S_j the enthalpy and the entropy of the jth component at operation temperature and pressure, H_0 and S_0 the enthalpy and entropy of the jth component at environment temperature and pressure and T_0 the temperature of the environment. The thermodynamic properties $(H_j - H_0)$ and $(S_j - S_0)$ for CO_2 and H_2 were calculated using the NIST Webbook (NIST Chemistry Webbok, 2020). In the case of $NaHCO_3$, Na_2CO_3, NaOH, H_2CO_3 and HCOONa, these parameters $(H_j - H_0)$ and $(S_j - S_0)$ were not considered as the mass fraction of these solutes in the aqueous streams is always below 0.03 (see Table 1) and therefore the contribution of the enthalpy and entropy of these solutes can be safely neglected. The properties of the water were calculated using Water97_v13.xla,

Table 1
Temperature, pressure and mass and energy balances of the streams of the reduction of CO_2 in the form of $NaHCO_3$ into formate according to Fig. 1.

Stream	1	2	3	4	5	6	7	8	9	10	11	12	13
P (bar)	1	200	200	200	200	200	200	200	200	200	1	1	1
T (°C)	25	25	277	25	275	301	301	301	45	35	39	39	39
Substance (kg/s)													
$NaHCO_3$	0.53	0.53	0.53	–	0.53	0.15	6.0E−03	0.15	0.15	0.15	0.13	–	0.13
Na_2CO_3	–	–	–	–	–	–	–	–	–	–	0.01	–	0.01
NaOH	–	–	–	–	–	–	–	–	–	–	8.5E−06	–	8.5E−06
H_2CO_3	–	–	–	–	–	–	–	–	–	–	1.7E−04	–	1.7E−04
CO_2	–	–	–	–	–	–	–	–	–	–	2.0E−04	1.9E−04	3.7E−06
H_2O	5.2	5.2	5.2	–	5.2	5.2	0.19	5.0	5.0	5.0	5.0	6.8E−03	5.0
Zn	–	–	–	0.62	0.62	–	–	–	–	–	–	–	–
HCOONa	–	–	–	–	–	0.30	0.01	0.29	0.29	0.29	0.29	–	0.29
ZnO	–	–	–	–	–	0.77	0.77	–	–	–	–	–	–
H_2	–	–	–	–	–	1.0E−02	3.8E−04	9.7E−03	9.7E−03	9.7E−03	9.7E−03	9.7E−03	7.2E−06
Total (kg/s)	5.8	5.8	5.8	0.62	6.4	6.4	1.0	5.4	5.4	5.4	5.4	0.02	5.4
ΔH (kW)													
$NaHCO_3$	0	0	0	0	0	0	0	0	0	0	0	–	0
Na_2CO_3	–	–	–	–	–	–	–	–	–	–	0	–	0
NaOH	–	–	–	–	–	–	–	–	–	–	0	–	0
H_2CO_3	–	–	–	–	–	–	–	–	–	–	0	–	0
CO_2	–	–	–	–	–	–	–	–	–	–	2.4E−03	2.3E−03	4.4E−05
H_2O	0	96	5840	–	5780	6370	241	6130	500	295	296	0.41	296
Zn	–	–	–	0	63	–	–	–	–	–	–	–	–
HCOONa	–	–	–	–	–	0	0	0	0	0	0	–	0
ZnO	–	–	–	–	–	120	120	–	–	–	–	–	–
H_2	–	–	–	–	–	42	1.6	40	3.8	2.4	1.9	1.9	1.4E−03
ΔH Total (kW)	0	96	5840	0	5840	6530	363	6170	504	298	298	2.3	296
ΔS (kW/ K)													
$NaHCO_3$	0	0	0	0	0	0	0	0	0	0	0	–	0
Na_2CO_3	–	–	–	–	–	–	–	–	–	–	0	–	0
NaOH	–	–	–	–	–	–	–	–	–	–	0	–	0
H_2CO_3	–	–	–	–	–	–	–	–	–	–	0	–	0
CO_2	–	–	–	–	–	–	–	–	–	–	7.8E−06	7.7E−06	1.4E−07
H_2O	0	−0.03	14	–	14	15	0.6	14	1.3	0.65	1.0	1.3E−03	1.0
Zn	–	–	–	5.3E−04	0.15	–	–	–	–	–	–	–	–
HCOONa	–	–	–	–	–	0	0	0	0	0	0	0	0
ZnO	–	–	–	–	–	0.28	0.28	–	–	–	–	–	–
H_2	–	–	–	–	–	−0.12	−4.7E−03	−0.12	−0.20	−0.21	6.3E−03	6.3E−03	4.7E−06
ΔS Total (kW/K)	0	−0.03	14	5.3E−04	14	15	0.83	14	1.1	0.44	1.0	7.7E−03	1.0

which is an Add-In for MS Excel based on the industrial standard IAPWS-IF97 (Wagner and Pruß, 2002).

For the solid compounds, Zn and ZnO, the value of C_{pj} varies with temperature as stated in Table S1 (Perry et al., 1997). In this case, the differences $H_j - H_0$ and $S_j - S_0$ were calculated with Eqs. (7) and (8):

$$H_j - H_0 = \int_T^{T_0} C_{pj} dT \tag{7}$$

$$S_j - S_0 = \int_T^{T_0} \frac{C_{pj}}{T} dT \tag{8}$$

Chemical exergy ($\dot{E}_{ch}$) was calculated using Eq. (9) (Kotas, 2012).

$$\dot{E}_{ch} = \sum_j \dot{n}_j \left(\sum_j x_j \tilde{e}_{0j} + \tilde{R} T_0 \sum_J x_j ln x_j \right) \tag{9}$$

where $\dot{n}_j$ is the molar flow rate (kmol/s) of each current, $\tilde{e}_{0j}$ is the molar chemical exergy (J/mol) of the jth component, $\tilde{R}$ the molar gas constant (8.3144 J/mol K), T_0 the temperature of the environment. The standard chemical exergy ($\tilde{e}_0$) of the species involved in the hydrothermal conversion of $NaHCO_3$ into HCOONa at standard conditions ($t_0 = 25$ °C and $P_0 = 1.013$ bar) can be found in Table S2 (Kotas, 2012).

The value of the standard chemical exergy of HCOONa and H_2CO_3 were not tabulated, and therefore, it was necessary to calculate them using Eq. (10) (Kotas, 2012):

$$\tilde{e}^0_{compound} = \Delta G^0_f + \sum E^0_{el} \tag{10}$$

where E^0_{el} is the standard chemical exergy of the constituent elements, ΔG^0_f is the standard molar Gibbs energy of formation, whose values are gathered in Table S3 (Dean, 1979; Reid et al., 2001). HCOONa and H_2CO_3 are produced according to reactions R4 and R5 respectively:

$$NaOH\ (aq) + CO\ (g) \rightarrow HCOONa\ (aq) \tag{R4}$$

$$CO_2\ (g) + H_2O\ (l) \rightarrow H_2CO_3(aq) \tag{R5}$$

To evaluate the exergy destruction in the cooler (C-1), it was necessary to calculate the physical exergy of the water using as cooling fluid. In the cooler, the inlet temperature was fixed at 20 °C, while the outlet temperature was 25 °C, considering that the mass flow of cooling water was 4000 kg/h. The $\dot{E}_{ph}$ was calculated according to Eq. (6). The thermodynamic properties of water were calculated with the MS Excel Add-In Water97v13.xla (Wagner and Pruß, 2002).

The exergy efficiency (ψ) is defined as the ratio of the useful exergy in each unit of the process and the exergy supplied to the system. It is calculated by Eq. (11) (Martín et al., 2006):

$$\psi = \frac{\dot{E}_{useful}}{\dot{E}_{input}} \tag{11}$$

Table 2
Exergy balances and equations for the calculation of the exergy destruction rate according to Eq. (3) and exergetic efficiency according to Eq. (11).

Unit	Exergy balance	Exergy efficiency
[a]Pump (P-1)	$\dot{E}_1 + \dot{W}_{P1} - \dot{E}_2 = \dot{E}_{D,P1}$	$\psi_{P1} = \frac{\dot{E}_2 - \dot{E}_1}{\dot{W}_{U1}}$
Heat exchanger (E-1)	$(\dot{E}_2 - \dot{E}_3) + (\dot{E}_8 - \dot{E}_9) = \dot{E}_{D,E1}$	$\psi_{E1} = \frac{\dot{E}_3 - \dot{E}_2}{\dot{E}_8 - \dot{E}_9}$
Mixed valve (V-1)	$\dot{E}_3 + \dot{E}_4 - \dot{E}_5 = \dot{E}_{D,V1}$	–
Reactor (R-1)	$\dot{E}_5 - \dot{E}_6 = \dot{E}_{D,R1}$	–
Cooler (C-1)	$(\dot{E}_9 - \dot{E}_{10}) + (\dot{E}_{CW,in} - \dot{E}_{CW,out}) = \dot{E}_{D,C1}$	$\psi_{C1} = \frac{\dot{E}_{10} + \dot{E}_{CW,out}}{\dot{E}_9 + \dot{E}_{CW,in}}$
Expansion valve (V-2)	$\dot{E}_{10} - \dot{E}_{11} = \dot{E}_{D,V2}$	–

[a]$\dot{W}_{P1}$ = 235 kW was calculated with ASPEN ONE V.10 simulation software for an efficiency of 0.6 for the pump and 0.9 for the driver.

where $\dot{E}_{useful}$ is the sum of the useful exergy flows leaving the unit and $\dot{E}_{input}$ the sum of the exergy of all streams entering each unit of the process.

The exergetic improvement potential rate (*IP*) of each unit of the plant is calculated according to Eq. (12) (Mojarab Soufiyan et al., 2016).

$$IP = (1 - \psi)\left(\dot{E}_{in} - \dot{E}_{out}\right) \tag{12}$$

In addition to the exergetic improvement potential rate, the sustainability index (*SI*) factor was also used to evaluate the environmental impact of a process due to the exergy destruction. The parameter *SI* is the relation between the input exergy and the exergy losses of the system (Eq. (13)). The higher *SI*, the lower the environmental impact factor (Castro et al., 2018):

$$SI = \frac{1}{1 - \psi} \tag{13}$$

The exergy balances applied to calculate the exergy destruction rate and the equations used for calculating the exergetic efficiency of each unit of the process in the continuous synthesis of formate from $NaHCO_3$ (Fig. 1) are gathered in Table 2. It is important to highlight that the exergy balances were not applied to the cyclone S-1 and the flash chamber S-2, since these are separation units in which there are neither change in the temperature or pressure nor input of external work. Therefore, there is no exergy destruction in these units. Moreover, they can be considered as part of the previous units, this is, the cyclone S-1 as the separation part of the reactor R-1 and the flash chamber S-2 as the separation unit of the depressurization valve V-2. In regard to the exergetic efficiency, it was only calculated for the pump P-1, the heat exchanger E-1 and the cooler C-1. Mixer valve V-1 has no efficiency associated since mixing is a process that takes place spontaneously when substances are put into physical contact (Kotas, 2012). Likewise, there is no definition for the efficiency in the reactor R-1 where an exothermic reaction takes place, nor for the expansion valve (Kotas, 2012).

4. Exergoeconomic analysis

The exergoeconomic balance can be described with Eq. (14) (Aghbashlo et al., 2019):

$$c_{in}\dot{E}_{in} + c_w\dot{W} + \dot{Z} = c_{out}\dot{E}_{out} \tag{14}$$

where c is the unit exergoeconomic cost (€/kJ), $\dot{E}$ is the exergy of the stream (kJ/h), $\dot{W}$ is the electrical work (kJ/h) and $\dot{Z}$ the investment cost rate (€/h). Table 3 gathers the exergoeconomic balances calculated with Eq. (14) for each unit of the process according to Fig. 1.

To calculate the unit exergoeconomic cost of each stream it is necessary to solve the system of linear equations resulting from Table 3. In order to solve the system, the following assumptions must be considered: in the heat exchanger E-1 the cost per exergy unit on the hot stream remains constant and therefore $c_8 = c_9$. In the separation units, the following auxiliary equations can be assumed $c_7 = c_8$ and $c_{12} = c_{13}$ (Mahmoudi et al., 2016). In the valves V-1 and V-2, the investment cost rate $\dot{Z}$ can be considered negligible. The value of c_w can be calculated considering the price of electricity. The values of c_{H_2O}, c_1 and c_4 can be calculated with Eq. (15) since these are streams entering the system (Aghbashlo et al., 2019):

$$c_{input} = \frac{\sum_j \dot{m}_{j,in} C_{j,in}}{\sum_j \dot{m}_{j,in} e_{0j,in}} \tag{15}$$

where $\dot{m}$ is the mass flow of the jth component (kg/h), C its cost (€/kg) and e_0 its standard chemical exergy (kJ/kg).

The investment cost rate ($\dot{Z}$) of the process unit was calculated according to Eq. (16) (Aghbashlo et al., 2019):

$$\dot{Z} = \frac{Z \cdot CRF \cdot \phi}{H} \tag{16}$$

where Z is the investment cost (€), *CRF* the capital recovery factor calculated by Eq. (17), ϕ the maintenance factor with a supposed value of 1.06 and H the annual working hours. In this work, the selected value for H was 8000 h.

$$CRF = \frac{i(1+i)^N}{(1+i)^N - 1} \tag{17}$$

where i is the interest rate and in this case it was supposed to be 10% and N is the operation unit life time (supposed value, $N = 20$ year).

The cost associated to the irreversibility produced in each process unit is defined by Eq. (18) (Aghbashlo et al., 2019):

$$\dot{C}_D = c_u\dot{E}_D \tag{18}$$

where $\dot{E}_D$ is the exergy destruction in each unit and c_u is the exergoeconomic cost associated with each piece of equipment of the plant. This cost per unit of exergy loss was calculated according to Eq. (19) (Aghbashlo et al., 2019):

$$c_u = \frac{c_{in}\dot{E}_{in} + c_w\dot{W}}{\dot{E}_{in} + W} \tag{19}$$

The total exergoeconomic cost rate of each unit of the continuous process is given by Eq. (20) (Aghbashlo et al., 2019):

$$\dot{C}_T = \dot{Z} + c_u\dot{E}_D \tag{20}$$

The capital cost of the main units of this process were calculated with the methodology detailed in a previous work of this research group (Quintana-Gómez et al., 2021). The cost of each piece of equipment updated to present costs with the Chemical Engineering Plant Cost Index 2019 (CEPCI=607.5) (Chemengonline, 2019) are included in Table 4.

Table 3
Exergoeconomic balances for each plant unit calculated with Eq. (14).

Unit	Balance
Pump (P-1)	$c_1\dot{E}_1 + c_w\dot{W} + \dot{Z}_{P-1} = c_2\dot{E}_2$
Heat exchanger (E-1)	$c_2\dot{E}_2 + c_8\dot{E}_8 + \dot{Z}_{E-1} = c_3\dot{E}_3 + c_9\dot{E}_9$
Valve (V-1)	$c_3\dot{E}_3 + c_4\dot{E}_4 + \dot{Z}_{V-1} = c_5\dot{E}_5$
Reactor (R-1)	$c_5\dot{E}_5 + \dot{Z}_{R-1} = c_6\dot{E}_6$
Hydrocyclone (S-1)	$c_6\dot{E}_6 + \dot{Z}_{S-1} = c_7\dot{E}_7 + c_8\dot{E}_8$
Cooler (C-1)	$c_9\dot{E}_9 + c_{cH2O,in}\dot{E}_{cH2O,in} + \dot{Z}_{C-1} = c_{10}\dot{E}_{10} + c_{cH2O,out}\dot{E}_{cH2O,out}$
Expansion valve (V-2)	$c_{10}\dot{E}_{10} + \dot{Z}_{V-2} = c_{11}\dot{E}_{11}$
Flash chamber (S-2)	$c_{11}\dot{E}_{11} + \dot{Z}_{S-2} = c_{12}\dot{E}_{12} + c_{13}\dot{E}_{13}$

Table 4
Capital cost of the main units of the process according to Fig. 1.

Unit	Cost (€)
Reactor (R-1)	450500
Pump (P-1)	42130
Heat exchanger (E-1)	56170
Cooler (C-1)	27590
Cyclone (S-1)	4026
Flash chamber (S-2)	4730

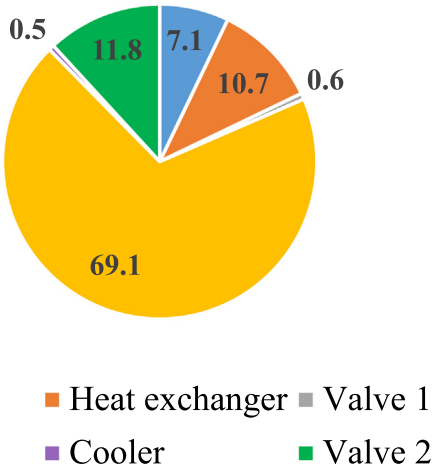

Fig. 2. Percentage of exergy loss of each equipment respect to the total exergy loss of the process.

Regarding the operation, it is worthy to highlight that as the bicarbonate is generated by the capture of CO_2 on NaOH, its cost was considered the same as that of NaOH, that has a price of 353 €/t (Echemi, 2021), whereas the cost considered for Zn was 2201 €/t (MarketsInsider, 2021). It was assumed the plant would be located at Valladolid area (Spain) where the overall price of industrial water would be approximately 1.9 €/t (Aquavall, 2021), and the cost of industrial electricity is on average 0.075 €/kWh (Aura Energía, 2021).

5. Results and discussion

Exergy results

Table 5 gathers the value of the exergy of each stream involved in the process. The exergy destruction loss and the efficiency for each piece of equipment calculated with the equations gathered in Table 2 are shown in Table 6. It also shows the improvement potential rate calculated according Eq. (12) and the environmental impact factor *SI* calculated with Eq. (13). It is clear from Table 6 that the highest exergy destruction rate took place in the reactor, reaching 1268 kW. This unit presented also the highest exergetic improvement potential rate, with an improvement value of 220 kW. The pump (P-1) also presented a significant improvement rate of 73 kW, while the energy destruction rate was 131 kW. The depressurization valve (S-2) showed also a significant destruction rate of 217 kW. In regard to the lowest destruction rates, they were observed in the cooler (C-1) and mixer valve (V-1), with values of 10 kW and 11 kW, respectively. The total exergy destruction rate per kg of CO_2 was 6600 kJ/kg treated CO_2, where the contribution of the reactor was higher than 4500 kJ/kg treated CO_2. In terms of the produced sodium formate, the total exergy destruction rate was 6260 kJ/kg of formate produced.

The exergy destruction in the reactor is almost 70% of the total exergy destruction in the plant, as it is shown in Fig. 2. Therefore, in order to improve the exergetic performance of the plant, the reactor is the unit that must be considered at the first place. The exergy destruction in the reactor can be ascribed to the chemical reactions that take place. In the heat exchanger and valve 2, the exergy destruction was also significant, representing 11% and 10% respectively of the total destruction. The exergy destruction in valve 1 and in the cooler was <1%, and therefore, these units do not need further optimization in terms of exergy performance.

In terms of exergetic efficiency, as one might have expected, the pump showed the lowest efficiency ratio with a value of 0.44, due to the fact that it used the high quality electrical work for pumping the feed stream (Mojarab Soufiyan et al., 2016). On the other hand, the cooler had an efficiency ratio of 1 (Table 6), as it was considered that there was no heat loss and the amount of water was selected to fulfill the ideal performance of the unit. This means that after passing the cooler the energy is still completely available to conduct other process duties (Mojarab Soufiyan et al., 2016).

The higher the sustainability index, the lower the environmental impact, since the higher the efficiency the higher the *SI* (Castro et al., 2018). The *SI* values varied from 1.8 to *ca.* 10, being the pump the equipment with the highest environmental impact.

As aforementioned, the reactor was the unit with the highest exergy destruction rate. In order to investigate the effect of the reaction yield in the exergy destruction, other two different reaction yields were simulated, specifically yields to sodium formate of 35% and 95%. For the lower yield, the total destruction rate per kg of treated CO_2 decreased to 4960 kJ/kg treated CO_2. However, as due to the low yield the quantity of formate produced was lower, the exergy destruction rate in terms of product synthesized increased to 9530 kJ/kg of formate. On the contrary, as one might expect, when the yield increased to 95%, the total exergy destruction rate decreased to 5300 kJ/kg of formate. As it is clear for Table 7, when the yield was reduced to 35%, the exergy destruction rate in the reactor decreased to 808 kW and when the conversion into formate was near complete, the destruction rate of the exergy increased to 1570 kW. The percentage of the

Table 5
Exergy rate for each stream involved in the reduction of $NaHCO_3$ into formate. Streams were numerated according to Fig. 1.

Stream	1	2	3	4	5	6	7	8	9	10	11	12	13
$\dot{E}$ (kW)	2250	2354	3969	3343	7301	6033	600	5433	3621	3611	3394	1140	2254

Table 6
Exergy destruction rate, exergetic efficiency, *IP* and *SI* for the process units according to Fig.

1.UNIT	$\dot{E}_D$ (kW)	Efficiency	*IP* (kW)	*SI*
Pump (P-1)	131	0.44	73	1.8
Heat exchanger (E-1)	197	0.89	21	9.2
Valve (V-1)	11	–	–	–
Reactor (R-1)	1268	0.83	220	5.8
Cooler (C-1)	10	1.00	–	–
Valve (V-2)	217	–	–	–

Table 7
Exergy destruction rate (kW) as a function of the yield to formate.

UNIT	Yield: 35%	Yield: 95%
Pump (P-1)	131	131
Heat exchanger (E-1)	179	210
Valve (V-1)	11	11
Reactor (R-1)	808	1570
Cooler C-1	10	10
Valve (V-2)	240	148

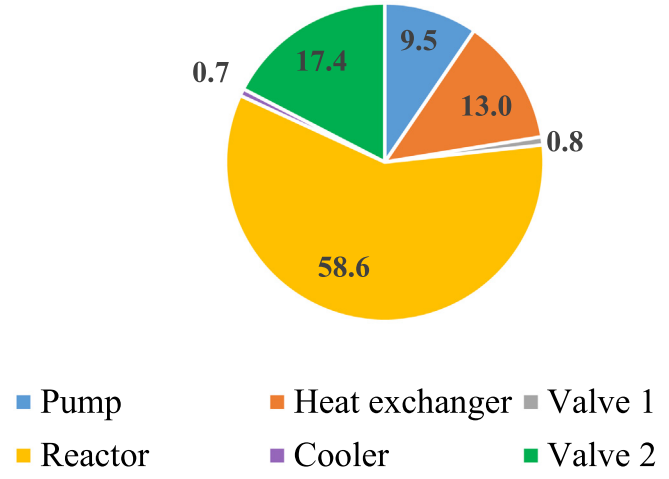

Fig. 3. Percentage of exergy loss of each equipment respect to the total exergy loss of the process for a yield to formate of 35%.

exergy destruction in the reactor with respect to the total exergy destruction was 59% and 76% when the yield was 35% and 95% respectively as plotted in Figs. 3 and 4.

Exergoeconomic results

In Table 8, the calculated values for the unit exergoeconomic costs of each stream based on the balances of Table 3, are gathered. The streams with highest exergoeconomic unit cost were 11, 12 and 13, which are the streams present in the flash separation unit. It is also important to highlight that the cost of stream 3 has a negative value of −0.25 €/MJ, which indicates that additional costs can be associated with this stream.

Table 9 summarizes the exergoeconomic results of a continuous plant for the hydrothermal production of formic acid from CO_2. It specifically tabulates costs associated to the exergy destruction in each unit ($\dot{C}_D$) calculated with Eq. (18), the exergy destruction rate ($\dot{E}_D$) calculated with the expressions gathered in Table 2, the factor c_u (Eq. (19)) and data from Table 7, the investment cost rate ($\dot{Z}$) calculated with Eq. (16) and the exergoeconomic cost rate of each unit ($\dot{C}_T$) calculated with Eq. (20).

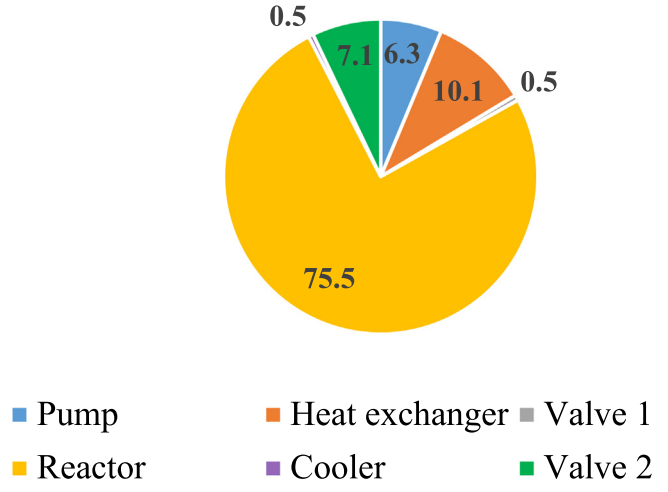

Fig. 4. Percentage of exergy loss of each equipment respect to the total exergy loss of the process for a yield to formate of 95%.

As previously described, an interest rate of 10% was considered for these calculation. As a complement, table S4 of the supporting information presents the results considering other values of the interest rate.

It is interesting to note that the highest cost factor (c_u) was observed in the flash chamber with a value of 1.15 €/MJ, which is in agreement with the results of Table 7, where the highest unitary exergoeconomic cost where found in the streams involved in the separation in the flash chamber. Despite this high exergoeconomic cost, as in the flash chamber there is no exergy destruction, the total exergy cost associated is given only by the investment cost rate ($\dot{Z}$), showing a low value of 0.1 €/h. The highest total exergoeconomic cost rate was identified in the reactor, since it also presented the highest destruction rate. The total exergoeconomic cost in the reactor had a calculated value of 1636 €/h and represented the 67% of the total exergoeconomic cost rate of the process (Fig. 5). The other process units with significant total exergoeconomic cost rates were the heat exchanger and the pump, with values of 624 and 183 €/h respectively. Only these three units constituted >99.5% of the total exergoeconomic costs. As one might expect, those units where the destruction rate was null, showed a negligible $\dot{C}_T$ value due to the fact that the total cost only included the investment cost rate ($\dot{Z}$). The contribution of these units, the hydrocyclone and the flash chamber to the total exergoeconomic cost rate was near zero, and therefore, they are not plotted in Fig. 5. In the case of the cooler, it was neither considered in Fig. 5, because its contribution to the overall cost rate was lower than 0.1%. According to Fig. 5, for a yield of 71%, the heat exchanger represented 25.5% and the pump 7.5% of the total exergoeconomic cost rate. The total exergoeconomic cost was 2.4 €/kg of treated CO_2 and 2.3 €/kg of produced formate.

Considering the volatility of the price of electricity in the current context, Table S5 of the supplementary information presents the results obtained for different values of this price. It can be noted that the price of electricity has a relatively low impact on the cost of the process, as electricity is only used to power the liquid pump. This cost is comparatively small with respect to the cost of raw materials, and particularly Zn, which is the dominating cost of the process (Quintana-Gómez et al., 2021).

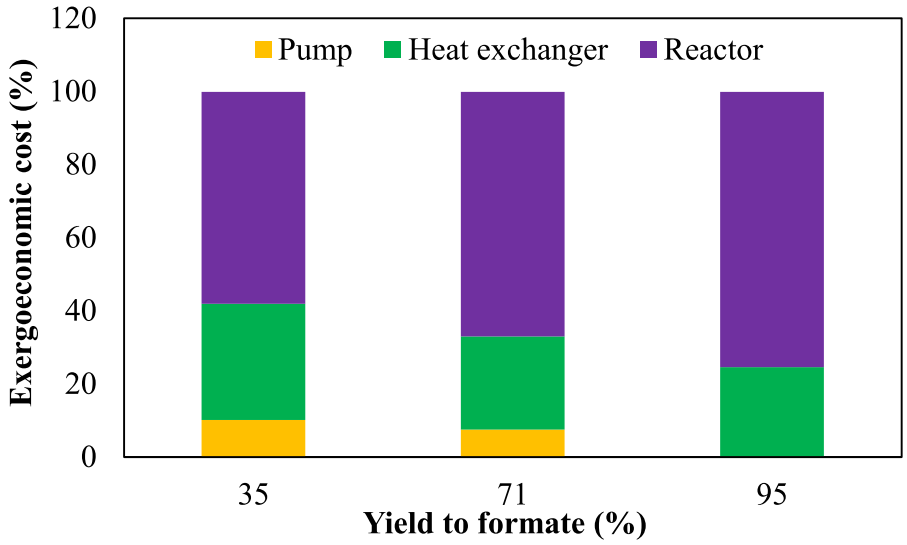

Fig. 5. Percentage contribution to the total exergoeconomic cost rate of the pump, heat exchanger and reactor in the continuous plant for the hydrothermal synthesis of formate from CO_2 at different formate yields.

Table 8
Unitary exergoeconomic cost factor for each stream involved in the process of CO_2 hydrothermal reduction into formate according to Fig. 1.

Stream	1	2	3	4	5	6	7	8	9	10	11	12	13
c (€/MJ)	0.42	0.41	−0.25	1.1	0.36	0.43	1.1	1.1	1.1	1.1	1.2	1.2	1.2

Table 9
Cost factor (c_u), the exergy destruction rate ($\dot{E}_D$), the cost associated to the destruction rate ($\dot{C}_D$), the investment cost rate ($\dot{Z}$) and the exergoeconomic cost rate ($\dot{C}_T$) for the process units according to Fig. 1.

Unit	c_u (€/MJ)	$\dot{E}_D$ (MJ/h)	$\dot{C}_D$ (€/h)	Z (€/h)	$\dot{C}_T$ (€/h)
Pump	0.39	471	182	0.66	183
Heat exchanger	0.88	710	623	0.87	624
Reactor	0.36	4564	1629	7.0	1636
Hydrocyclone	0.43	–	–	0.06	0.06
Cooler	0.07	36	3	0.43	3.2
Flash chamber	1.2	–	0	0.07	0.07

When the yield to formate was reduced from 71% to 35%, the contribution of the reactor to the total exergoeconomic cost rate decreased to 58% while the contribution of the heat exchanger and the pump increased to 32 and 10% respectively (Fig. 5). On the contrary, when the yield to formate increased to 95%, the contribution of the reactor to the total exergoeconomic cost increased to 75%, while the contribution of the pump dropped to less than 0.03% and its contribution cannot be appreciated in Fig. 5. The total exergoeconomic costs were 3.5 and 2.7 €/kg of produced formate for a formate yield of 35% and 95% respectively. In both cases, the total costs were higher than in the case of a yield of 71% that showed a value of 2.3 €/kg of formate. It could be expected that for a yield of 95%, the cost would decrease due to the higher quantity of formate produced. However, the increase of the exergoeconomic cost in the reactor cannot be compensated by the increase in the production of formate.

6. Conclusions

In this work, an exergy and exergoeconomic performance assessment of a continuous process for the production of formate from CO_2 was conducted. The exergy destruction rate was of 6600 kJ/kg treated CO_2 and 6260 kJ/kg formate. The reactor showed the major contribution to the exergy destruction rate, reaching a value of 1268 kW. The exergy destruction rate per kg of treated CO_2 was 6600 kW/kg CO_2. The effect of the formate yield in the exergy destruction rate was also investigated, concluding that when the yield increased from 71% to 95%, the exergy destruction rate of the reactor related to the total exergy destruction of the process increased from 70% to 76%, while when the yield is reduced to 35%, the contribution of the reactor also decreased to 59%. Likewise, when the exergoeconomic analysis was performance, the unit with a highest contribution to the total exergoeconomic cost rate of the process was also the reactor, exhibiting the 67% of the total exergoeconomic cost rate. The total exergoeconomic cost rate per kg of produced formate was 2.3 €while treated CO_2 costed 2.4 €/kg from the point of view of exergoeconomic cost.

CRediT authorship contribution statement

Laura Quintana-Gómez: Investigation, Writing – original draft. **José J. Segovia:** Conceptualization, Methodology, Validation. **Ángel Martín:** Conceptualization, Methodology, Validation, Writing – review & editing, Supervision, Funding acquisition. **M. Dolores Bermejo:** Conceptualization, Writing – review & editing, Supervision, Project administration, Funding acquisition.

Declaration of competing interest

The authors declare that they have no known competing financial interests or personal relationships that could have appeared to influence the work reported in this paper.

Data availability

No data was used for the research described in the article.

Acknowledgments

This work/project was supported by the Regional Government of Castilla *y* León, Spain and the EU-FEDER program, Spain through project CLU-2019-04 and by the Ministry of Science and Universities, Spain through project RTI2018-097456-B-I00.

Appendix A. Supplementary data

Supplementary material related to this article can be found online at https://doi.org/10.1016/j.egyr.2022.09.065.

References

Aghbashlo, M., Tabatabaei, M., Rastegari, H., Ghaziaskar, H.S., 2019. Optimization of continuous glycerol esterification with acetic acid based on exergoeconomic and exergoenvironmental approaches. Sustain. Prod. Consum. 17, 62–73. http://dx.doi.org/10.1016/j.spc.2018.09.008.

Alami, A.H., Abu Hawili, A., Tawalbeh, M., Hasan, R., Al Mahmoud, L., Chibib, S., Mahmood, A., Aokal, K., Rattanapanya, P., 2020. Materials and logistics for carbon dioxide capture, storage and utilization. Sci. Total Environ. 717, 137221. http://dx.doi.org/10.1016/j.scitotenv.2020.137221.

Anwar, M.N., Fayyaz, A., Sohail, N.F., Khokhar, M.F., Baqar, M., Yasar, A., Rasool, K., Nazir, A., Raja, M.U.F., Rehan, M., Aghbashlo, M., Tabatabaei, M., Nizami, A.S., 2020. CO2 utilization: Turning greenhouse gas into fuels and valuable products. J. Environ. Manag. 260 (January), 110059. http://dx.doi.org/10.1016/j.jenvman.2019.110059.

Aquavall, 2021. Tarifas abastecimiento agua. http://aquavall.es/wp-content/uploads/2017/06/tarifas_agua_2017.pdf. (Accessed 20 January 2021).

Aura Energía, 2021. Tarifas luz industria pení. https://www.aura-energia.com/tarifas-luz-industria-peninsula/. (Accessed 20 January 2021).

Castro, M., Román, C., Echegaray, M., Mazza, G., Rodriguez, R., 2018. Exergy analyses of onion drying by convection: Influence of dryer parameters on performance. Entropy 20 (5), 1–9. http://dx.doi.org/10.3390/e20050310.

Chemengonline, 2019. Chemical engineering plant cost index annual average. https://www.chemengonline.com/2019-chemical-engineering-plant-cost-index-annual-average/. (Accessed 15 January 2021).

De Guido, G., Compagnoni, M., Pellegrini, L.A., Rossetti, I., 2018. Mature versus emerging technologies for CO2 capture in power plants: Key open issues in post-combustion amine scrubbing and in chemical looping combustion. Front. Chem. Sci. Eng. 12 (2), 315–325. http://dx.doi.org/10.1007/s11705-017-1698-z.

Dean, J.A., 1979. Lange's HandBook of Chemistry, twelfth ed. McGraw-Hill.

Dincer, I., Rosen, M., 2020. Exergy, Energy, Environment and Sustainable Develoment, third ed. Elsevier.

Dowlati, M., Aghbashlo, M., Mojarab Soufiyan, M., 2017. Exergetic performance analysis of an ice-cream manufacturing plant: A comprehensive survey. Energy 123, 445–459. http://dx.doi.org/10.1016/j.energy.2017.02.007.

Duo, J., Jin, F., Wang, Y., Zhong, H., Lyu, L., Yao, G., Huo, Z., 2016. NaHCO3-enhanced hydrogen production from water with Fe and in situ highly efficient and autocatalytic NaHCO3 reduction into formic acid. Chem. Commun. 52 (16), 3316–3319. http://dx.doi.org/10.1039/c5cc09611a.

Echemi, 2021. Caustic soda price analysis. https://www.echemi.com/productsinformation/pd20150901041-caustic-soda-pearls.html. (Accessed 20 January 2021).

Ferrer, S., Mezquita, A., Aguilella, V.M., Monfort, E., 2019. Beyond the energy balance: Exergy analysis of an industrial roller kiln firing porcelain tiles. Appl. Therm. Eng. 150 (December 2018), 1002–1015. http://dx.doi.org/10.1016/j.applthermaleng.2019.01.052.

Gomez, L.Q., Shehab, A.K., Al-Shathr, A., Ingram, W., Konstantinova, M., Cumming, D., McGregor, J., 2020. H2-free synthesis of aromatic, cyclic and linear oxygenates from CO2. ChemSusChem 13 (3), 647–658. http://dx.doi.org/10.1002/cssc.201902340.

Jin, F., Zeng, X., Liu, J., Jin, Y., Wang, L., Zhong, H., Yao, G., Huo, Z., 2014. Highly efficient and autocatalytic H2O dissociation for CO2 reduction into formic acid with zinc. Sci. Rep. 4, 1–8. http://dx.doi.org/10.1038/srep04503.

Jovan, D.J., Dolanc, G., 2020. Can green hydrogen production be economically viable under current market conditions. Energies 13 (24), 6599. http://dx.doi.org/10.3390/en13246599.

Keith, D.W., Holmes, G., St Angelo, D., Heidel, K., 2018. A process for capturing CO2 from the atmosphere. Joule 2 (8), 1573–1594. http://dx.doi.org/10.1016/j.joule.2018.05.006.

Kotas, T.J., 2012. The Exergy Method of Thermal Plant Analysis. Exergon Publishing Company.

Kothandaraman, J., Goeppert, A., Czaun, M., Olah, G.A., Surya Prakash, G.K., 2016. CO2 capture by amines in aqueous media and its subsequent conversion to formate with reusable ruthenium and iron catalysts. Green Chem. 18 (21), 5831–5838. http://dx.doi.org/10.1039/c6gc01165a.

Mac Dowell, N., Fennell, P.S., Shah, N., Maitland, G.C., 2017. The role of CO2 capture and utilization in mitigating climate change. Nature Clim. Change 7 (4), 243–249. http://dx.doi.org/10.1038/nclimate3231.

Mahmoudi, S.M.S., Pourreza, A., Akbari, A.D., Yari, M., 2016. Exergoeconomic evaluation and optimization of a novel combined augmented Kalina cycle/gas turbine-modular helium reactor. Appl. Therm. Eng. 109, 109–120. http://dx.doi.org/10.1016/j.applthermaleng.2016.08.011.

Mardini, N., Bicer, Y., 2021. Direct synthesis of formic acid as hydrogen carrier from CO2 for cleaner power generation through direct formic acid fuel cell. Int. J. Hydrogen Energy 46 (24), 13050–13060. http://dx.doi.org/10.1016/j.ijhydene.2021.01.124.

MarketsInsider, 2021. Zinc commodity. https://Markets.Businessinsider.Com/Commodities/Zinc-Price. (Accessed 20 January 2021).

Martín, C., Villamañán, M.A., Chamorro, C.R., Otero, J., Cabanillas, A., Segovia, J.J., 2006. Low-grade coal and biomass co-combustion on fluidized bed: Exergy analysis. Energy 31 (2–3), 330–344. http://dx.doi.org/10.1016/j.energy.2005.01.008.

Michalkiewicz, B., Koren, Z.C., 2015. Zeolite membranes for hydrogen production from natural gas: State of the art. J. Porous Mater. 22 (3), 635–646. http://dx.doi.org/10.1007/s10934-015-9936-6.

Mojarab Soufiyan, M., Aghbashlo, M., Mobli, H., 2017. Exergetic performance assessment of a long-life milk processing plant: A comprehensive survey. J. Clean. Prod. 140, 590–607. http://dx.doi.org/10.1016/j.jclepro.2015.11.066.

Mojarab Soufiyan, M., Dadak, A., Hosseini, S.S., Nasiri, F., Dowlati, M., Tahmasebi, M., Aghbashlo, M., 2016. Comprehensive exergy analysis of a commercial tomato paste plant with a double-effect evaporator. Energy 111, 910–922. http://dx.doi.org/10.1016/j.energy.2016.06.030.

NIST Chemistry Webbok, 2020. Thermophysical properties of fluid systems. https://webbook.nist.gov/chemistry/fluid/. (Accessed 2 October 2020).

Perry, R.H., Green, D.W., O'Hara Maloney, J., 1997. Perry's Chemical Engineers' HandBook. McGraw-Hill.

Petrakopoulou, F., Tsatsaronis, G., Boyano, A., Morosuk, T., 2011. Exergoeconomic and exergoenvironmental evaluation of power plants including CO2 capture. Chem. Eng. Res. Des. 89 (9), 1461–1469. http://dx.doi.org/10.1016/j.cherd.2010.08.001.

Quintana-Gómez, L., Martínez, L., Román-González, D., Segovia, J.J., Martín, Á., Bermejo, M.D., 2021. Energy and economic analysis of the hydrothermal reduction of CO 2 into formate. Ind. Eng. Chem. Res. http://dx.doi.org/10.1021/acs.iecr.1c01961.

Reid, R.C., Prausnitz, J.M., Poling, B.E., 2001. Propierties of Gases and Liquides, fifth ed. McGraw-Hill Education.

Roman-Gonzalez, D., Moro, A., Burgoa, F., Pérez, E., Nieto-Márquez, A., Martín, Á., Bermejo, M.D., 2018. 2Hydrothermal CO 2 conversion using zinc as reductant: Batch reactio, modeling and parametric analysisof the process. J. Supercrit. Fluids 140 (May), 320–328. http://dx.doi.org/10.1016/j.supflu.2018.07.003.

Styring, P., Jansen, D., de Coninck, H., Reith, H., Armstrong, K., 2011. Carbon capture and utilisation in the green economy. In: Centre for Low Carbon Futures.

Takahashi, H., Kori, T., Onoki, T., Tohji, K., Yamasaki, N., 2008. Hydrothermal processing of metal based compounds and carbon dioxide for the synthesis of organic compounds. J. Mater. Sci. 43 (7), 2487–2491. http://dx.doi.org/10.1007/s10853-007-2041-8.

Terehovics, E., Veidenbergs, I., Blumberga, D., 2017. Energy and exergy balance methodology. Wood chip dryer. Energy Procedia 128, 551–557. http://dx.doi.org/10.1016/j.egypro.2017.09.008.

Wagner, W., Pruß, A., 2002. The IAPWS formulation 1995 for the thermodynamic properties of ordinary water substance for general and scientific use. J. Phys. Chem. Ref. Data 31 (2), 387–535. http://dx.doi.org/10.1063/1.1461829.

Xu, C., Xin, T., Li, X., Li, S., Sun, Y., Liu, W., Yang, Y., 2019. A thermodynamic analysis of a solar hybrid coal-based direct-fired supercritical carbon dioxide power cycle. Energy Convers. Manag. 196 (June), 77–91. http://dx.doi.org/10.1016/j.enconman.2019.06.002.

Yoo, M., Han, S.J., Wee, J.H., 2013. Carbon dioxide capture capacity of sodium hydroxide aqueous solution. J. Environ. Manag. 114, 512–519. http://dx.doi.org/10.1016/j.jenvman.2012.10.061.

Yusuf, A., Giwa, A., Mohammed, E.O., Mohammed, O., Hajaj, A.Al., Abu-Zahra, M.R.M., 2019. CO2 utilization from power plant: A comparative techno-economic assessment of soda ash production and scrubbing by monoethanolamine. J. Clean. Prod. 237, 117760. http://dx.doi.org/10.1016/j.jclepro.2019.117760.